Aspects of the Correlation between Sodar and Mast Instrument Winds

STUART BRADLEY

Physics Department, University of Auckland, Auckland, New Zealand

(Manuscript received 1 December 2012, in final form 7 May 2013)

ABSTRACT

On a uniform terrain site, differences between a sodar and a mast-mounted cup anemometer will arise because of turbulent fluctuations and wind components being measured in different spaces, and because of the inherent difference between scalar and vector averaging. This paper develops theories for turbulence-related random fluctuations resulting from finite sampling rates and sampling from spatially distributed volumes. Coefficients of determination (R^2) are predicted comparable to those obtained in practice. It is shown that more than two-thirds of the reduction in R^2 arises from differences in the winds measured by mast instruments and by sodars, rather than by sodar errors: both instruments are measuring accurately, but just not in the same place or at the same time. The result is that sodars being used operationally should be able to measure winds to a root-mean-square accuracy of around 2%.

1. Introduction

The quality of remote sensing instruments is generally judged by performing an intercomparison experiment (e.g., Antoniou et al. 2004). Winds are measured at several heights by cup or sonic anemometers on a mast, together with measurements by a remote sensing instrument. What do the reported correlation values mean in terms of predicting differences in measured wind speed? This question arises since these differences between cup anemometers and remote sensing instruments are the essence of whether remote sensing gives ''bankable'' data. What quality of wind measurements can be expected from remote sensing in a typical installation? This is relevant since intercomparisons are often under test conditions unlike those typically encountered at normal sites.

Some previous intercomparison experiments have touched on the spatial and temporal separation issues treated in detail below. Mastrantonio and Fiocco (1982) describe transmission on three acoustic beams simultaneously, with emphasis on Doppler processing, rather than the effects of spatial separation of their beams. Contini et al. (2006) consider ultrasonic anemometers, with some interesting observations about spatial separation of sensors, but the scales and other considerations are different from those of sodars. Contini et al. (2007) show improvements from one sodar over another if all acoustic beams are transmitted simultaneously, but the comparison is between two very different sodar systems. Other works (e.g., Contini et al. 2004) consider poor sodar setup: in the work below it is assumed that such factors are negligible.

2. Correlation between mast and remote instruments

For simplicity in the following, the mean wind U is toward the $+x$ direction and variations in wind vector components are (u, v, w). A scatterplot is obtained from N measurements of mast instrument wind speed $U_{m,n}$ and the corresponding remote instrument wind speed $U_{r,n}$, where $n = 1, 2, \ldots, N$. Neither of the measurement pairs, $U_{m,n}$ and $U_{r,n}$, necessarily is equal to the actual wind U_n which includes the turbulent fluctuations, because all instruments exhibit measurement errors. However, it is conventional to consider the mast measurements as error free, whereas

$$U_{r,n} = U_n + \varepsilon_{r,n}, \tag{1}$$

where ε is Gaussian distributed with standard deviation σ_ε.

Corresponding author address: Stuart Bradley, Physics Department, University of Auckland, Private Bag 92019, Auckland, New Zealand.
E-mail: s.bradley@auckland.ac.nz

DOI: 10.1175/JTECH-D-12-00256.1

Since both mast and remote instruments are highly linear, a physically sensible model to use is a straight line, of the form

$$\hat{U}_{r,n} = aU_{m,n} + b \quad \text{or} \quad \hat{U}_{r,n} = aU_{m,n}. \tag{2}$$

This describes the best remote instrument estimate $\hat{U}_{r,n}$ if a measurement $U_{m,n}$ is made at the mast. A measure of the scatter around the best-fit line is the coefficient of determination R^2, where

$$R^2 = 1 - \frac{\sum_{n=1}^{N} (U_{r,n} - \hat{U}_{r,n})^2}{\sum_{n=1}^{N} (U_{r,n} - \overline{U_r})^2} \approx 1 - \frac{\sum_{n=1}^{N} (U_{r,n} - U_{m,n})^2}{\sum_{n=1}^{N} (U_n - U)^2}. \tag{3}$$

The approximation is valid since for these instruments a is very close to 1 and b is very close to 0. It is convenient to write R^2 as

$$R^2 = 1 - \frac{\left(\frac{\Delta U_{\rm rms}}{U}\right)^2}{\left(\frac{\sigma_U}{U}\right)^2}, \tag{4}$$

where

$$\Delta U_{\rm rms} = \left[\frac{1}{N}\sum_{n=1}^{N} (U_{r,n} - U_{m,n})^2\right]^{1/2} = \sqrt{\frac{1}{N}\sum_{n=1}^{N} \varepsilon_{r,n}^2} = \sigma_\varepsilon \tag{5}$$

is the root-mean-square (rms) difference between mast-measured and remote-measured wind speed, and

$$U = \frac{1}{N}\sum_{n=1}^{N} U_n \quad \text{and}$$
$$\sigma_U^2 = \frac{1}{N}\sum_{n=1}^{N} (U_n - U)^2 \tag{6}$$

are the mean and variance of the wind speed over the measurement intercomparison period ($N \gg 1$), respectively. Quantity σ_U^2 arises from diurnal and synoptic variations and should not be confused with the short-term fluctuations due to turbulence.

The Weibull probability distribution function is commonly used to model the probability, $p(U)dU$, of observing a wind speed between U and $U + dU$, written as

$$p(U) = \frac{k}{\lambda}\left(\frac{U}{\lambda}\right)^{k-1} e^{-(U/\lambda)^k}. \tag{7}$$

The ratio σ_U/U depends only on the shape parameter k via

$$\left(\frac{\sigma_U}{U}\right)^2 = \frac{\Gamma(1 + 2/k)}{\Gamma^2(1 + 1/k)} - 1. \tag{8}$$

The rms difference $\Delta U_{\rm rms}$ can arise from a number of causes, including differences between scalar (cup type) and vector (remote type) measurements; remote sensing sampling over spatially distributed volumes; sampling spread over time; and spatial separation between the remote sensing volumes and the mast sensor. Except in the case of complex terrain, these differences are essentially random instead of systematic and are a result of turbulent fluctuations in wind speed being sensed differently by the mast sensors and the remote sensors. Systematic differences occur in complex terrain (Bingol et al. 2009; Behrens et al. 2012; Bradley et al. 2012; Bradley 2012). It is assumed that instrumentation is setup carefully so problems such as poor alignment are not an issue.

Clearly, R^2 is not a property of the remote sensing instrument alone. It depends on moments U and σ_U^2 of the wind regime in which the intercomparisons were completed. If the site is uniform, if turbulence intensity is very low, and if wind speeds are widely distributed, then a very high R^2 should be achieved by any good-quality sodar or lidar remote sensing instrument, since the inherent limitations of the instrument are being reached. This essentially explains why it is possible to get very high R^2 values in some intercomparisons, while much lower values are obtained in others.

Figure 1 shows the relationship between $\Delta U_{\rm rms}/U$ and R^2 for a range of wind regimes. For $\sigma_U/U = 0.52$ (Weibull $k = 2$), the fractional rms wind difference is 6% for an intercomparison producing $R^2 = 0.985$, or 4% for an $R^2 = 0.995$. These results are also checked by simulating a large number ($N = 1000$) of random mast winds from a Weibull distribution using

$$U_n = \lambda[-\ln(1 - r_n)]^{1/k}, \tag{9}$$

where r_n are random numbers uniformly distributed between 0 and 1. For each mast wind, a remote instrument wind is generated with an additional random normally distributed variation having standard deviation σ_ε. The results of this stochastic simulation are shown as crosses in Fig. 1 for $\sigma_U/U = 0.6$ ($k = 1.72$).

3. Cup-sodar differences due to turbulence

A cup anemometer measures the total wind run in a sampling period, whereas a remote sensing instrument averages the vector wind components measured during

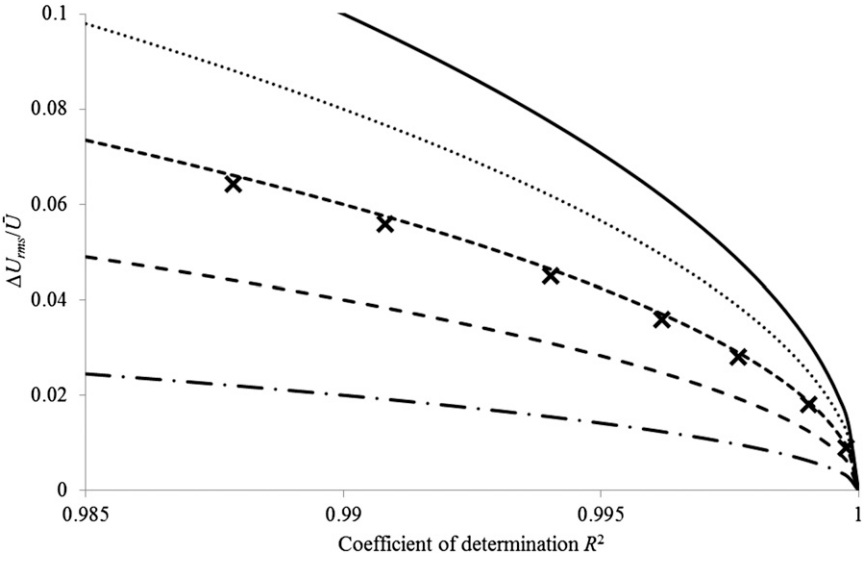

FIG. 1. The normalized rms difference in wind speed $\Delta U_{\rm rms}/U$ recorded by two instruments, and its relationship to R^2 obtained from a straight-line regression. The curves are for $\sigma_U/U = 1$ (solid line), 0.8 (dotted line), 0.6 (short dashes), 0.4 (long dashes), and 0.2 (dotted–dashed). The crosses are from a stochastic simulation with $\sigma_U/U = 0.6$.

a sampling period. Kristensen (1999) has described the bias arising from these different methods of measuring wind, as follows.

The wind speed measured by a cup anemometer is $U_{m,n} = [(U_n + u_n)^2 + v_n^2]^{1/2}$, whereas a remote sensing instrument measures the vector $(U_n + u_n, v_n, w_n)$, albeit via three or more separate measurements. The average wind speed measured by the mast-mounted cup anemometer is (to the second order)

$$\overline{U_m} = \frac{1}{N}\sum_{n=1}^{N} U_{m,n} = \frac{U}{N}\sum_{n=1}^{N}\left(1 + 2\frac{u_n}{U} + \frac{u_n^2}{U^2} + \frac{v_n^2}{U^2}\right)^{1/2} \approx U + \frac{\frac{1}{N}\sum_{n=1}^{N} v_n^2}{2U}, \tag{10}$$

whereas that measured by a remote sensing instrument is $\overline{U_r} = U$. The normalized mean difference between mast and remote measured winds is

$$\frac{\overline{U_m} - \overline{U_r}}{U} = \frac{1}{2}\left(\frac{\sigma_v}{U}\right)^2. \tag{11}$$

The term in brackets is the transverse turbulent intensity (not to be confused with σ_U/U), and the difference in measured wind speeds is typically 0%–2%.

The work of Kristensen (1999) summarized above did not describe the random differences arising from scalar versus vector averaging. For a particular turbulence intensity, these two different measures of wind speed will contribute to the scatter in a plot of winds measured by mast instruments versus winds measured by remote instruments. This scatter derives from the variance in the difference $U_m - U_r$. For cup measurements

$$\sigma_m^2 = \frac{1}{N}\sum_{n=1}^{N}(U_{m,n} - \overline{U_m})^2 \approx \sigma_u^2 \tag{12}$$

and for remote measurements

$$\sigma_r^2 = \frac{1}{N}\sum_{n=1}^{N}(U + u_n - U)^2 = \sigma_u^2. \tag{13}$$

The variance of the difference is

$$\begin{aligned}\Delta U_{\rm rms}^2 &= \frac{1}{N}\sum_{n=1}^{N}(U_{r,n} - U_{m,n})^2 \\ &= \frac{1}{N}\sum_{n=1}^{N}[(U_{r,n} - U) - (U_{m,n} - U)]^2 \\ &= \frac{1}{N}\sum_{n=1}^{N}(U_{r,n} - U)^2 + \frac{1}{N}\sum_{n=1}^{N}(U_{m,n} - U)^2 \\ &= \sigma_m^2 + \sigma_r^2 = 2\sigma_u^2,\end{aligned} \tag{14}$$

assuming the two instrument errors are uncorrelated and that $\sigma_m^2 = \sigma_r^2 = \sigma_u^2$. The second assumption is based on the variance from the sodar being derived from the spectral width (the turbulent spectrum well sampled) and on background acoustic noise not corrupting spectral

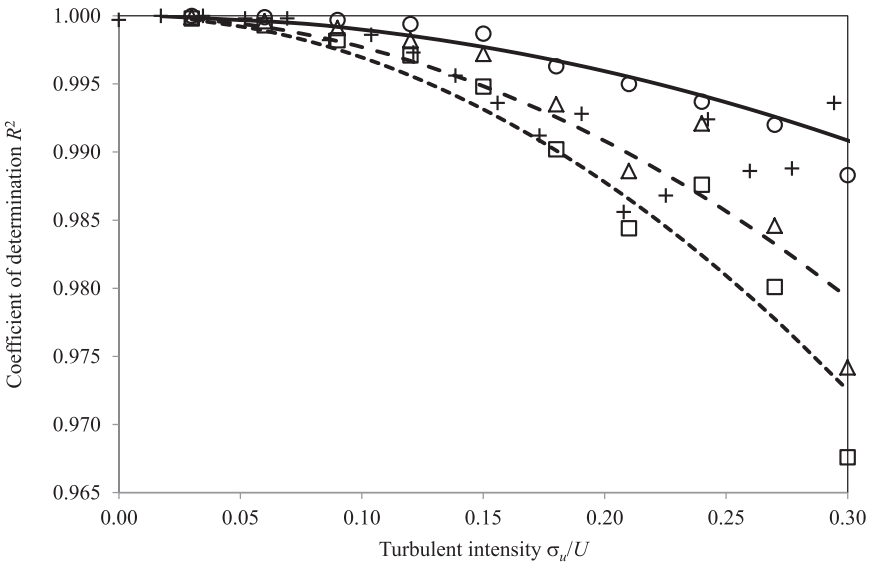

FIG. 2. The effect of turbulent intensity σ_u/U on R^2. The predicted variation based on scalar–vector averaging differences (solid line) and a stochastic simulation of that effect (circles). The triangles are from a stochastic simulation of the effect of an 80-m separation between mast and sodar, and the long dashes is a line of best fit. The squares are from a simulation of the effect of the time delay between sampling each of the three radial velocity components in a three-beam sodar, and short dashes are the line of best fit. The crosses are based on data given in Moore and Bailey (2006).

estimates. The effects of combining data from different beams are not included here.

Wind measurements are typically averaged over 10 min. For a sodar having a vertical range of 300 m, this average is typically over 72 wind estimates. The result is a reduction in the variance of 72, assuming Gaussian-distributed variations, giving

$$\frac{\Delta U_{\text{rms}}}{U} \approx \frac{1}{\sqrt{72}} \frac{\sqrt{2}\sigma_u}{U} = \frac{1}{6}\frac{\sigma_u}{U}. \tag{15}$$

The normalized standard deviation of the discrepancy between mast- and remote-measured winds is therefore proportional to the turbulence intensity, and the scatter naturally affects R^2. We can simulate this by generating winds U from random Weibull deviates, and then generating random u_n, v_n, and w_n values for a succession of samples at this U. These turbulent components are generated by filtering a white noise spectrum to obtain a von Kármán velocity spectrum using the method described by the company MathWorks, based on Careta et al. (1993) and Ewert (2008). Results are shown in Fig. 2 and compared with the prediction from (15). Weibull parameters $k = 2$ and $\lambda = 8\,\text{m s}^{-1}$ are used. A height of 80 m is chosen for the generation of u_n, v_n, and w_n and both simulated mast winds and simulated sodar winds are averaged over 10 min. Fitting a straight line to the resulting scatterplot from 1000 stochastic 10-min winds gives R^2 values for each chosen turbulence intensity value.

Depending on the site, a sodar can receive reflections from fixed nonatmospheric objects. Consequently, sodar–mast intercomparisons are inevitably conducted with the sodar placed 80 m or more from the mast. This introduces a further difference between the sodar-measured wind and the mast-sensed winds, since the same volume of air is not being sensed. Figure 2 shows the effect on R^2 of a mast–sodar separation of $D = 80$ m. In this case the u_n, v_n, and w_n are sampled for the random mast winds and delayed samples used for the sodar winds, with delay $D/U = 11.4$ s in this example. Since the time constant for autocorrelation of the turbulent velocity components is around 20 s, the mast samples and the sodar samples are quite different. A similar procedure is followed as for the scalar–vector averaging example, using the same parameters, giving the data points shown as triangles in Fig. 2 and the accompanying line of best fit. Note that this procedure also includes the scalar–vector averaging differences, which account for about half of the reduction in R^2.

A further cause of differences between winds recorded by mast instruments and sodars arises because three or more spatially separated volumes are successively sampled by the sodar, with time delays between each volume sampling (Bradley 2007). This effect can again be simulated using the random von Kármán method.

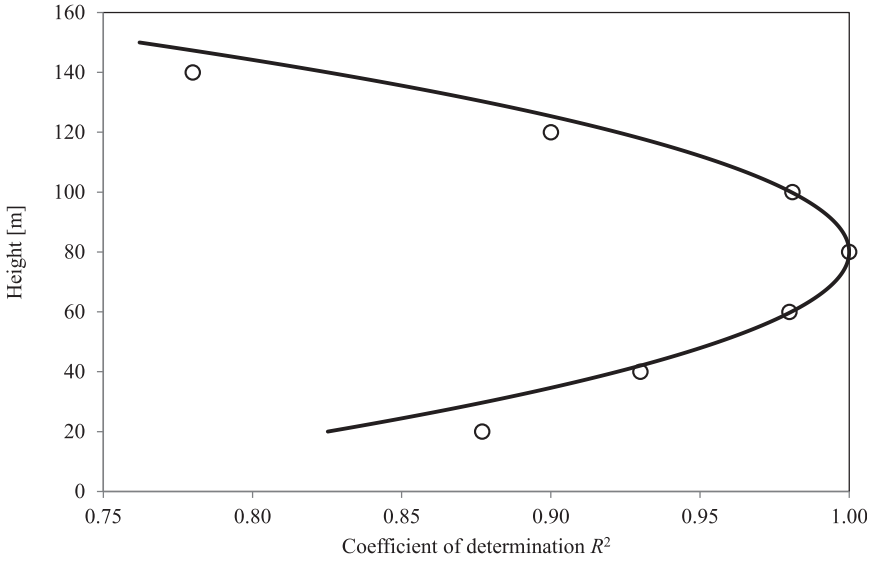

FIG. 3. The variation of R^2 with sampling height for a comparison between radial winds derived from two opposing beams in a five-beam sodar, based on Behrens et al. (2010). The solid line is the line of best fit assuming a quadratic dependence.

The scalar–vector effect and the mast–sodar separation effect are included, as described above. The time between sampling at height $h = 80$ m on one beam, and sampling at that height on the next beam, is taken to be 2.8 s. A three-beam sodar is simulated, with beams 1 and 2 in orthogonal planes and tilted at zenith angles of 18°, whereas beam 3 is vertical. Results are shown by squares in Fig. 2, together with the line of best fit.

Moore and Bailey (2006) presented a plot of measured differences between mast and sodar winds (equivalent to $\Delta U_{\rm rms}/U$) at a range of turbulent intensities. These data can be scaled and (4) used to obtain an equivalent R^2. The results are shown as crosses in Fig. 2 and, except at the highest turbulent intensities, agree well with the random von Kármán simulations. Note that the mast–sodar separation distance for the data from Moore and Bailey (2006) is not known, but 80 m is typical for such intercomparisons.

Remote sensing instruments measure the three wind vector components in orthogonal directions x, y, and z by solving equations that relate the wind components to the Doppler shift along each radial beam direction. As an example, a three-beam system having two beams tilted at angle θ off vertical and one vertical beam would solve equations such as

$$\begin{aligned} m_{n,1} &= (U + u_{n,1})\sin\theta + w_{n,1}\cos\theta, \\ m_{n,2} &= v_{n,2}\sin\theta + w_{n,2}\cos\theta, \quad \text{and} \\ m_{n,3} &= w_{n,3} \end{aligned} \tag{16}$$

(in this example, beam 1 is aligned with the wind), with solution

$$U_{r,n} = \frac{m_{n,1} - m_{n,3}\cos\theta}{\sin\theta} = U + u_{n,1} + (w_{n,1} - w_{n,3})/\tan\theta. \tag{17}$$

The m represent radial wind components estimated from measured Doppler shifts, and

$$\begin{aligned} \Delta U_{\rm rms}^2 &= \frac{1}{N}\sum_{n=1}^{N}(U_{r,n} - U)^2 + \frac{1}{N}\sum_{n=1}^{N}(U_{m,n} - U)^2 \\ &= \frac{1}{N}\sum_{n=1}^{N}[u_{n,1} + (w_{n,1} - w_{n,3})/\tan\theta]^2 + \sigma_u^2 \\ &= \frac{2\sigma_w^2}{\tan^2\theta} + \sigma_u^2 \\ &= \frac{\sigma_u^2}{\sin^2\theta} \end{aligned} \tag{18}$$

if $\sigma_w^2 = 0.5\sigma_u^2$. Because θ is small, the $1/\tan\theta$ dominates the first term on the right. This shows that the scatter in the speed measurement is prone to vertical turbulence in particular for small angle-tilted beams (small θ).

From Fig. 2 it is clear that, even in uniform terrain, the sampling of three or more spatially separated volumes by a sodar, over a time interval of something like 9 s or more, contributes to a reduced R^2. This effect has also been explored experimentally by Behrens et al. (2010). Figure 3, adapted from this work, shows the R^2 obtained

by comparing winds estimated from opposing beams on a five-beam Metek sodar. The beams, called here beam 1 and beam 2, are aligned with the wind with one tilted upwind by $\theta = 17.5°$ and the other downwind with the same zenith angle. The time between a sample from beam 1 and a sample from beam 2 at the same height is $\Delta t_{12} = 18$ s. A very high R^2 (effectively 1.00) is measured at the height where turbulence from one sampled volume has moved to the second sampled volume in the time Δt_{12}. The high R^2 is possible because the scalar–vector averaging difference is not present (both measurements are from the same sodar), and effectively the same turbulent volume is being sampled. Since sodars sample turbulent structure in a large volume, the different pointing angles of the two opposing beams is not a factor so that

$$\begin{aligned}\Delta U_{\mathrm{rms}}^2 &= \frac{1}{N}\sum_{n=1}^{N}(U_1 - U_2)^2 \\ &= \frac{1}{N}\sum_{n=1}^{N}(u_1 - u_2)^2 \\ &= \frac{1}{N}\sum_{n=1}^{N}u_1^2 - \frac{2}{N}\sum_{n=1}^{N}u_1u_2 + \frac{1}{N}\sum_{n=1}^{N}u_2^2 \\ &= 2\sigma_u^2(1-\rho_{12}). \end{aligned} \tag{19}$$

The correlation function between the upwind and downwind turbulent wind components can be approximated by

$$\begin{aligned}\rho_{12} &\approx e^{-[1/2(\Delta t/\tau)^2]} \\ &\approx 1 - \frac{1}{2\tau^2}\left(\frac{2z\tan\theta}{U} - \Delta t_{12}\right)^2, \end{aligned} \tag{20}$$

where $2z\tan\theta/U$ is the time the turbulence takes to advect from beam 1 to beam 2 at height z and at wind speed U, and τ is the turbulence correlation time (see, e.g., Blanc-Benon et al. 1991; Chu et al. 1996). The first-order linearized approximation of the exponential will likely only be valid close to height giving maximum R^2. From (4),

$$R^2 = 1 - A(z - z_{\max})^2, \tag{21}$$

where

$$z_{\max} = \frac{U\Delta t_{12}}{2\tan\theta} \tag{22}$$

and

$$A = \left(\frac{2\sigma_u\tan\theta}{\sigma_U U\tau}\right)^2. \tag{23}$$

The data plotted in Fig. 3 are fitted using (21) to find $z_{\max}$ and A. From $z_{\max}$ and the known θ and Δt_{12}, an estimate of $U = 2.8\,\mathrm{m\,s^{-1}}$ is obtained. The turbulent intensity and σ_U are not known. But if values of $\sigma_u/U = 0.2$ and $\sigma_U/U = 0.22$ (or $k = 5.2$) are assumed, then $\tau = 29 \pm 1$ s is obtained, equal to $z_{\max}/U = 29$ s, which would be expected if the integral length scale is assumed to be equal to $z_{\max}$. Such a narrow Weibull could occur because the experiment by Behrens et al. (2010) had a duration of only seven days. The explanation of Fig. 3 in terms of advection of turbulence therefore seems plausible.

4. Conclusions

Given the above discussed differences between mast and sodar, what is the best current estimate of the fundamental wind speed errors in a sodar? The commonly quoted R^2 values for remote sensing instruments are *not* a property of the instrument, but are more closely associated with how the intercomparison experiment is carried out. Very high values of the coefficient of determination, R^2, are now reported for lidar comparisons with mast instruments (Mikkelsen and Bradley 2011), providing the data are filtered to remove turbulent fluctuation and other environmental effects. The difficulty with doing this for sodars is that the signals originate from turbulence. This means that filtering data from an intercomparison experiment to retain only low-turbulence data will necessarily mean a low signal-to-noise ratio for the sodar, and a corresponding reduction in R^2 resulting from statistical errors in finding the Doppler spectrum's peak position.

There is real difficulty therefore in answering the question: How good is a sodar? Most field use, away from the idealized ''laboratory'' environment, seems to have an R^2 value of 0.975–0.985. From Fig. 1, this corresponds to a range of relative difference, compared to a cup anemometer, of around 6%. However, from Fig. 2 it is seen that only about one-third of the R^2 reduction is due to the inescapable difference between scalar and vector averaging, and the remaining two-thirds of R^2 loss is attributable to measurement methodology, rather than errors. Both the mast instruments and the sodar are measuring winds accurately, but just not in the same place and at the same time. This suggests that sodars being used operationally can be expected to have real rms errors of around 2% (i.e., one-third of the 6% identified in Fig. 1).

Acknowledgments. The author is grateful to Torben Mikkelsen for the useful discussions.

REFERENCES

Antoniou, I., H. E. Jørgensen, S. von Hünerbein, S. G. Bradley, D. Kindler, G. Warmbier, and M. de Noord, 2004: The Profiler Intercomparison Experiment (PIE). *Proc. European Wind Energy Conf. and Exhibition,* London, United Kingdom, EWEA, CD-ROM.

Behrens, P., S. Bradley, and T. Wiens, 2010: A multisodar approach to wind profiling. *J. Atmos. Oceanic Technol.,* **27,** 1165–1174.

——, J. O'Sullivan, R. Archer, and S. Bradley, 2012: Underestimation of mono-static sodar measurements in complex terrain. *Bound.-Layer Meteor.,* **143,** 97–106.

Bingol, F., J. Mann, and D. Foussekis, 2009: Conically scanning lidar error in complex terrain. *Meteor. Z.,* **18,** 189–195.

Blanc-Benon, P., D. Juvé, and G. Comte-Bellot, 1991: Occurrence of caustics for high-frequency acoustic waves propagating through turbulent fields. *Theor. Comput. Fluid Dyn.,* **2,** 271–278.

Bradley, S. G., 2007: *Atmospheric Acoustic Remote Sensing.* CRC Press/Taylor and Francis Group, 328 pp.

——, 2012: A simple model for correcting sodar and lidar errors in complex terrain. *J. Atmos. Oceanic Technol.,* **29,** 1717–1722.

——, Y. Perrott, and A. Oldroyd, 2012: Corrections for wind-speed errors from sodar and lidar in complex terrain. *Bound.-Layer Meteor.,* **143,** 37–48.

Careta, A., F. Sagues, and J. M. Sancho, 1993: Stochastic generation of homogeneous isotropic turbulence with well-defined spectra. *Phys. Rev.,* **48E,** 2279–2287.

Chu, C. R., M. B. Parlange, G. G. Katul, and J. D. Albertson, 1996: Probability density functions of turbulent velocity and temperature in the atmospheric surface layer. *Water Resour. Res.,* **32,** 1681–1688.

Contini, D., G. Mastrantonio, A. Viola, and S. Argentini, 2004: Mean vertical motions in the PBL measured by Doppler sodar: Accuracy, ambiguities, possible improvements. *J. Atmos. Oceanic Technol.,* **21,** 1532–1544.

——, A. Donateo, and F. Belosi, 2006: Accuracy of measurements of turbulent phenomena in the surface layer with an ultrasonic anemometer. *J. Atmos. Oceanic Technol.,* **23,** 785–801.

——, F. M. Grasso, G. Mastrantonio, A. P. Viola, and P. Martano, 2007: Performances of a modular PC-based multi-tone sodar system in measuring vertical wind velocity. *Meteor. Z.,* **16,** 357–365.

Ewert, R., 2008: Broadband slat noise prediction based on CAA and stochastic: Sound sources from a fast random particle-mesh (RPM) method. *Comput. Fluids,* **37,** 369–387.

Kristensen, K., 1999: The perennial cup anemometer. *Wind Energy,* **2,** 59–75.

Mastrantonio, G., and G. Fiocco, 1982: Accuracy of wind velocity determinations with Doppler sodar. *J. Appl. Meteor.,* **21,** 820–830.

Mikkelsen, T., and S. G. Bradley, 2011: Lidar remote sensing. *Int. Sustainable Energy Rev.,* **5,** 19–23.

Moore, K. E., and B. H. Bailey, 2006: Maximizing the accuracy of sodar measurements for wind resource assessment. AWS Truewind Research Note 2, 10 pp. [Available online at http://www.awstruepower.com/2006/08/maximizing-the-accuracy-of-sodar-measurements-for-wind-resource-assessment/.]